



3D printed monoliths: From powder to an efficient catalyst for antibiotic degradation

S. Fernandez-Velayos^a, G. Vergara^a, J.M. Olmos^b, J. Sanchez-Marcos^a, N. Menendez^a, P. Herrasti^a, E. Mazarío^{a,*}

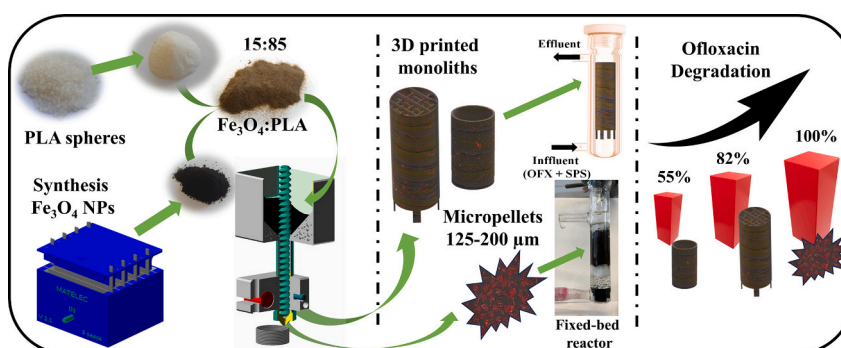
^a Departamento de Química Física Aplicada, Facultad de Ciencias, Universidad Autónoma de Madrid, 28049 Madrid, Spain

^b Departamento de Química Analítica, Facultad de Química, Universidad de Murcia, 30100 Murcia, Spain

HIGHLIGHTS

- The development of 3D catalyst from noncommercial filaments has been conducted.
- The powder blend is composed of 15 wt % of iron oxide and polylactic acid.
- Double mesh monolith design has improved the fluid dynamics of the process.
- Long-term experiments were conducted with excellent stability.
- Fixed-bed reactor configuration was used to totally degrade ofloxacin antibiotic.

GRAPHICAL ABSTRACT



ARTICLE INFO

Editor: Damià Barceló

Keywords:
Monoliths
3D technology
Wastewater continuous treatment
Emerging pollutants
Advanced oxidation processes

ABSTRACT

To improve the effectiveness and durability of wastewater treatment technologies, researchers are showing a growing interest in 3D printing technology. This technology has attracted significant interest owing to its ability to fabricate challenging complex geometries using different material compositions. This manuscript is focused on the development of 3D monoliths from noncommercial filaments, i.e., a powder blend of iron oxide and polylactic acid (PLA) at 15 wt% of the former. Different monolith designs have been prepared to improve the fluid dynamics of the process, so a simple cylinder (15-Fe₃O₄@PLA) and a cylinder with double the length and an internal mesh (15-Fe₃O₄@PLA-DM) were used. These monoliths were characterized by Scanning electron microscopy (SEM), Differential scanning calorimetry (DSC) and Mössbauer spectroscopy, then used for water-based ofloxacin degradation in a continuous down-up flow configuration. Additionally, computational fluid dynamics simulations were performed to estimate the degradation rate constants and analyze the distribution of fluid velocity and pollutant concentration along the 15-Fe₃O₄@PLA-reactor. The oxidant dose was also optimized to develop the highest degradation rate. The degradation of the target pollutant for those monoliths was 55 and 82 % under optimized conditions. In addition, the 15-Fe₃O₄@PLA-DM monolith was operated for long term experiments, keeping the degradation performance at a good 67 % for up to 120 h. Finally a fixed-bed reactor was mounted with printed pellets of the mixture (15:85), Fe₃O₄:PLA, after being ground in a range of 125–200 μm. Under this setup configuration, we observed the total degradation of ofloxacin. 3D printing technology is cheap,

* Corresponding author.

E-mail address: eva.mazario@uam.es (E. Mazarío).

<https://doi.org/10.1016/j.scitotenv.2023.167376>

Received 22 August 2023; Received in revised form 20 September 2023; Accepted 24 September 2023

Available online 25 September 2023

0048-9697/© 2023 The Authors. Published by Elsevier B.V. This is an open access article under the CC BY-NC-ND license (<http://creativecommons.org/licenses/by-nc-nd/4.0/>).

reproducible and time saving in the development of supported catalysts in comparison with conventional deposition techniques. Moreover, the leaching of active sites on streams was largely diminished. In fact under continuous operation the leached Fe concentration is below 0.1 ppm, corroborating the good adhesion of the catalyst in the PLA support.

1. Introduction

In recent decades, the consumption and disposal of pharmaceutical products has increased around the planet, generating adverse consequences for the quality of the environment (Bungau et al., 2021). Among those known as emerging pollutants, antibiotics are generating special attention due to their massive use and high self-consumption, causing a serious threat to human health, due to the proliferation of antimicrobial resistance (AMR). According to the WHO in its “aware” report (World Health Organization, n.d.-a, n.d.-b), the Watch antibiotic group includes those compounds that have higher resistance potential and/or that are at relatively high risk of selection of bacterial resistance, being recommended as essential first- or second-choice empiric treatment options for a limited number of specific infectious syndromes. Specifically, the target pollutant analyzed in this manuscript, ofloxacin, belongs to this group (Deng et al., 2022).

Despite the existing motivation to reduce the use of these antibiotics, there is no established environmental regulation to control and regulate pharmaceutical wastes. Antibiotics are only partially metabolized in the bodies of animals and humans, so they and their degradation byproducts reach wastewater treatment plants (WWTPs) with relative ease (Varela et al., 2014). Most WWTPs are not designed to efficiently remove them from wastewater, resulting in their discharge with concentrations that can reach up to $\mu\text{g/L}$, which allows for the dissemination of antimicrobial resistance to bacteria present in the natural environment. As has already been reported, antibiotic concentrations in both influent and effluent from WWTPs reach or exceed the predicted no-effect concentrations required for resistance selection (Alam et al., 2021).

Traditional wastewater treatment processes combine physical, chemical, and biological approaches for the removal of solids and organic matter. The primary treatment plant consists of aerobic biological processes, such as activated sludge processes, trickling filters or biofilters, oxidation ditches, and rotating biological contactors. In tertiary treatment, disinfection is mostly performed by chlorination. These traditional treatment methods have numerous shortcomings, such as low efficiency, sludge production, and the formation of potentially toxic byproducts. In addition, the subsequent incapacity to remove contaminants, such as residual antibiotic wastes, presents an extra challenge to these conventional processes. To overcome these drawbacks, advanced oxidation processes (AOPs) have started to generate great interest in the scientific community. AOPs are processes devoted to reducing pollutant concentrations in wastewater by in situ generation of hydroxyl or sulfate radicals (Kanakaraju et al., 2018)(Lee et al., 2020). These reactive species are the strongest oxidants that react unselectively once formed and contaminants will be quickly and efficiently fragmented and converted into smaller molecules and/or CO_2 . Hydroxyl and sulfate radicals are produced with the help of one or more primary oxidants (e.g., hydrogen peroxide, sodium persulfate) and/or energy sources (e.g., ultraviolet light, conventional heat or magnetic heating induction) (Liu et al., 2020a; Li et al., 2022b; Gallo-Cordova et al., 2021) or catalysts (e.g., metal oxides, (Liu et al., 2020b)), or the combination of catalyst and energy sources (Sayed et al., 2019; Liu et al., 2019).

At the laboratory scale, it is very common to use AOPs in batch mode, in which the catalyst is a bulk solid and the pollutant and oxidant are both added to the system, providing radical generation as well as pollutant degradation (Fernández-Velayos et al., 2023). The main drawback of this strategy is the implementation for the treatment of large water streams. On the other hand, advanced methodologies involving the use of supported catalysts on porous materials, such as

pillared clays, active carbon (Gupta and Garg, 2019), alumina (Cao et al., 2021), SiC, and ZrO_2 , (Nieto-Sandoval et al., 2021) enhance the efficiency of the process and especially the pollutant streams treated, whereby the volume of pollutant that can be degraded is significantly higher. The principal limitation in these systems is obtaining a durable anchorage or grafting of active catalyst on the porous support, which is crucial for the catalyst stability by hindering the deactivation by catalyst leaching (Zhu et al., 2020). In contrast to conventional manufacturing methods, 3D printing technology uses a fundamentally different approach in constructing a 3D structure via the sequential deposition of material layer-by-layer in a horizontal cross section. A wide range of materials can be utilized in 3D fabrication, which can be classified into three main categories: polymers, ceramics, and metals. In this context, 3D printing offers significant opportunities, such as flexibility in selecting materials, speed of manufacturing, optimized reactor configurations, fluid dynamics, and risk reduction (Jandyal et al., 2022). For example, activated carbon monoliths (ACm) fabricated by 3D printing have been applied for the adsorption and electrooxidation of antibiotics (Acuña-Bedoya et al., 2022). Recently, Cu_2O monoliths have been used for the degradation of ofloxacin (OFX), the antibiotic studied in the present work. These monoliths were obtained with a DLP 3D printer using a printable ink consisting of a mixture of teric and isopropyl alcohol (IPA) surfactants with Cu_2O microparticles at different doses (Xie et al., 2022). In other work, 3D graphene monoliths were manufactured using a direct ink writing technique known as Robocasting. In this case, the monoliths needed a postprinted treatment at 475°C in air to completely burn-out the ink residues, and afterward, they were sintered at 1200°C (Quintanilla et al., 2020). In a previous work, we printed 3D monoliths made from a commercial filament consisting of 43 wt% Fe microparticles and polylactic acid (PLA) as a matrix for tetracycline degradation (Fernández-Velayos et al., 2021). PLA is a relatively inexpensive material that costs between 15 and 20 US\$ per kg on average. The advantage of being a natural polymer makes PLA an eco-friendly material because of its low biodegradability and mechanical, thermal, and chemical resistance (Nasr Esfahani et al., 2021).

The main objective of this paper is to provide the first experimental trials of monolith preparation from powder mixtures with 3D printing technology. In this approach, the catalyst concentration and composition in the printable powder mixture can be tuned to improve the catalytic performance. An extended characterization study of the 3D monoliths was carried out in terms of composition, surface morphology and durability. AOPs were performed for different operating parameters, such as the inflow PDS concentration, and the configuration of the two different monoliths printed (simple and doble mesh) to provide a clear and argued qualitative description of the effect of those parameters in operating mode. Finally, sodium persulfate (SPS) activation for ofloxacin degradation with a fixed-fed column filled with millimetric $15\text{-Fe}_3\text{O}_4/\text{PLA}$ pellets was tested in log-term stream experiments.

2. Experimental setup

2.1. Materials and reagents

Sodium persulfate (SPS), ofloxacin (OFX), nitric acid, sodium hydroxide and glassy beads (2 mm) were purchased from Sigma Aldrich. Polylactic acid (PLA) spherical pellets were purchased from Smart Materials 3D. All the reagents mentioned above were used without further purification.

2.2. Electrochemical synthesis of magnetite

Magnetite synthesis has been carried out by the electrochemical process (Lozano et al., 2018). Briefly, a parallel electrode reactor with eight steel electrodes working as anodes and cathodes was used to carry out the electrochemical reaction, which resulted in the formation of magnetite. These reactions are produced by applying a current of 0.7 A to the system. An electrolytic sodium chloride aqueous solution (40 mM) is introduced into the reactor, which passes through the system in a continuous regime and is recirculated for 2 h with a flow rate of 30 mL/min, obtaining approximately 1 g of particles per hour of operation.

2.3. 3D monolith design and printing

The design of the different monoliths used was carried out using the

open-source software OpenScad, 2021-01. This program allows for easy and parameterized generation of complex repetitive structures, and it also enables exporting the model to an STL file without any gaps in both the surfaces and their joints. Two monoliths were designed: the first one is a simple cylinder with a height of 15 mm, a diameter of 7 mm, and a thickness of 1 mm (15-Fe₃O₄@PLA, Fig. 1a, and b). The second monolith consists of a cylinder with a height of 30 mm, a diameter of 12 mm, and a thickness of 0.5 mm. It has an internal mesh, depicted in Fig. 1c, which rotates 90 degrees every 0.94 mm, forming the structure shown in Fig. 1d,e; a schematic of the printed prototype is provided in Fig. 1f. The mesh has a thickness of 0.4 mm (15-Fe₃O₄@PLA – DM). The purpose of the mesh is to increase the catalyst surface area, disrupt laminar flow, and promote a more homogeneous mixture inside the reactor. The models were sliced using Cura 4.8 software, which provided us with an appropriate G-Code file for printing. The total weights of the 15-

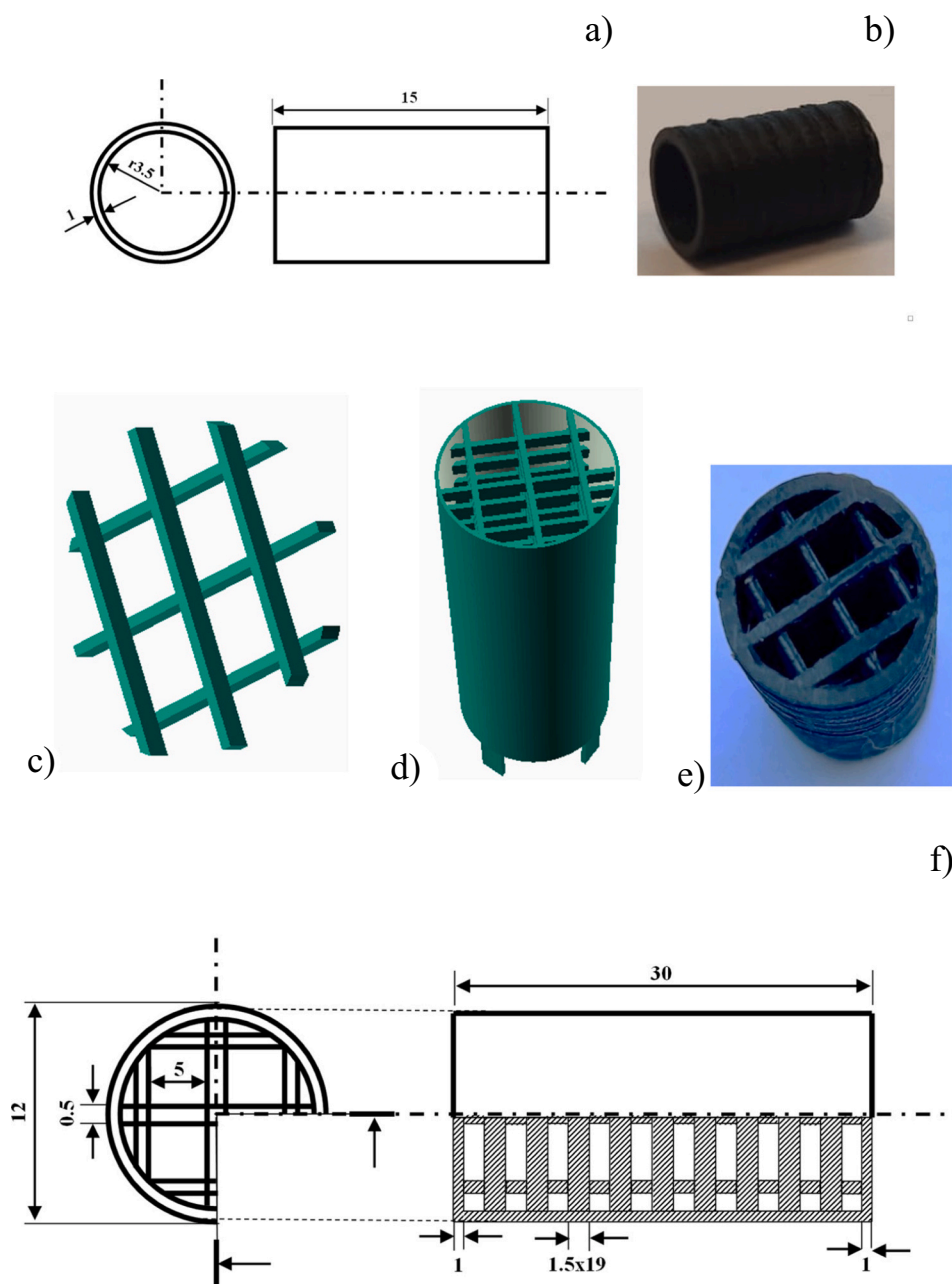


Fig. 1. a) Scheme of the single cylinder, 15-Fe₃O₄@PLA, (distances are shown in mm), b) printed single cylinder monolith, 15-Fe₃O₄@PLA, c) internal mesh of 15-Fe₃O₄@PLA – DM, d) entire monolith with internal mesh, 15-Fe₃O₄@PLA – DM, e) printed monolith, 15-Fe₃O₄@PLA – DM and, f) scheme of the printed 15-Fe₃O₄@PLA – DM (distances are shown in mm).

$\text{Fe}_3\text{O}_4@\text{PLA}$ and 15- $\text{Fe}_3\text{O}_4@\text{PLA}$ – DM monoliths were $W = 0.32 \pm 0.01$ g and $W = 2.0 \pm 0.2$ g, respectively.

The material used for printing these monoliths is a mixture of PLA and 15 % by weight of Fe_3O_4 nanoparticles. PLA acts as a support material, while magnetite serves as the catalyst. To achieve a homogeneous mixture, commercial PLA pellets from the SMART MATERIALS 3D brand were used. These pellets were placed in a blender for an average of 6–8 h, with a cycle of 2 min of blending followed by a 3-min rest period. The temperature was controlled to ensure that it did not exceed 45 °C. The resulting PLA powder was sieved through a 200 μm mesh and mixed with the appropriate proportion of Fe_3O_4 nanoparticles. This mixture was used for printing.

The monoliths were printed (see Fig. 1b and e) using a pellet extruder, specifically the Mahor XYZ extruder V4, mounted on an Ender 3 Pro 3D printer from Creality 3D Technology Co., Ltd. This extruder is capable of printing materials with a grain size smaller than 2 mm that can flow like sand. A 0.4 mm nozzle was used with an extruder temperature of 185 °C and a layer height of 0.2 mm, finally, the bed temperature was set to 50 °C.

The pellets packed in the fixed-bed reactor were obtained starting with printed pellets of 1 cm \times 1 cm with the same initial powder mixture $\text{Fe}_3\text{O}_4:\text{PLA}(15:85)$ and then milled in a CryoMill model CryoMill of Retsch brand, operated at -196 °C, with an agitation frequency of 30 Hz for 4 min. Then, the sample was sieved to obtain a fraction of micropellets in the range of 125 to 200 μm .

2.4. Experimental reactor configuration

AOP trials were performed in a glass tube (14 mm i.d., 70 mm length) immersed in a thermostated bath at 40 °C, with a fluid collector in the output side, and initial $\text{pH}_0 = 5$. Monoliths were placed in the center of the glass tube supported on a PLA blade. The experimental setup used in the fixed-bed reactor is shown in Fig. 2. Briefly, one gram of 15- $\text{Fe}_3\text{O}_4@\text{PLA}$ micropellets were immobilized between two layers of glass wool (5–10 mm). These three layers were placed above glassy beads (2 mm) and acts as a flow distributor. The fixed-bed reactor consists of an

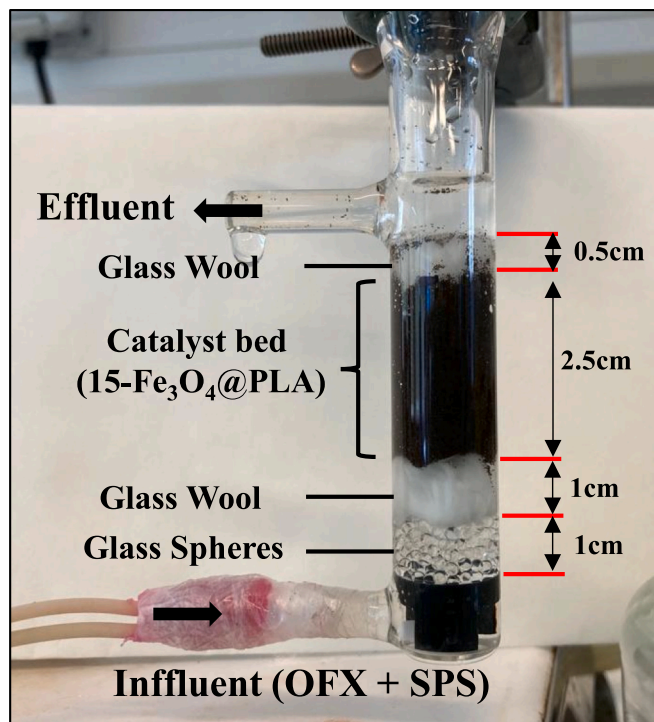


Fig. 2. Scheme of the fixed-bed reactors used in the AOP experiments packed with micropellets of 15- $\text{Fe}_3\text{O}_4@\text{PLA}$.

empty reactor volume of 6.36 mL and an empty bed volume of 1.8 mL corresponding to an experimental porosity equal to 0.28.

The adopted degradation parameters for the two configurations are as follows. The mixture of OFX and SPS at the desired concentrations was transferred to the reactor in an up-flow direction using a two-channel peristaltic pump, with an individual flow rate of 0.125 mL/min. The pH of the concentrated solutions of OFX and SPS was regulated to directly set a pH of 5 in the pollutant solution after mixing both reagents at the AOP initial time with a final concentration of 1 ppm OFX and 1 mM SPS. OFX degradation was analyzed by measuring the outflow OFX concentration at different times. All experiments were performed in triplicate, and the data are expressed as the mean \pm standard deviation.

2.5. Characterization techniques

Mössbauer spectroscopy was used to determine any change in the iron environment present in the 15- $\text{Fe}_3\text{O}_4@\text{PLA}$ ZVI@PLA monolith because of the higher temperatures reached during printing. The spectra were recorded at room temperature in triangular mode using a transmission spectrometer with a $^{57}\text{Co}/\text{Rh}$ source. Spectral analyses were performed by nonlinear fitting using the NORMOS program (Brand, 1987), and energy calibrations were accomplished with an $\alpha\text{-Fe}$ (6 μm) foil.

Particle Size Distribution (PSD) measurements were performed with MASTERSIZER-2000 equipment, which operates by means of laser diffraction (LD). It is equipped with a Hydro 2000/MU injection system that allows the dispersion of samples in fluids by turbine and ultrasound probe.

During the AOP reaction time, the OFX concentration was quantified using a high-performance liquid chromatograph (HPLC; Shimadzu ProminenceLC-2050 LT) equipped with a Diode Array detector (SPD-M30A) and a C-18 column (Eclipse Plus, 4.6×150 mm, 5 μm , Agilent) by an isocratic 85/15 % method of a mixture of 0.1 % v/v formic acid and acetonitrile as mobile phase with a flow rate of 0.7 mL/min at 25 °C. The injection volume was set at 10 μL , and 294 nm was chosen as the wavelength for OFX detection.

The iron composition of the monoliths and the possible Fe leaching from the catalyst during the degradation process were determined by inductively coupled plasma–optical emission spectrometry (ICP–OES) performed using Optima 2100 DV PerkinElmer equipment. Thus, a well-known volume of the solution was digested in 1 mL of aqua regia for 1 h and diluted to 10 mL with distilled water.

The morphological characterization and iron superficial analysis for the prototypes were carried out with both a Hitachi S-3000 N scanning electron microscope with 3 nm resolution at 25 kV equipped with a Wolfram filament with SE, BSE, and XFlash 6I30 detectors used for EDX analysis and a Chroma CL2 detector for cathodoluminescence and with Electron Beam Lithography eLINE-PLUS de Raith GmbH equipment.

Differential scanning calorimetry (DSC) was conducted using a DSC Discovery from TA Instruments under a nitrogen flux with a heating rate of 10 °C/min from 0 °C to 200 °C.

2.6. Computational fluid dynamics

The computational fluid dynamics (CFD) on the glass tube reactor were simulated with the finite element method using COMSOL Multiphysics® 5.6. The geometry of the reactor (see Fig. 2) was built from an STF file generated with the computer-aided design (CAD) software OpenScad and the CAD import module of COMSOL. Only the simple monolith was considered (15- $\text{Fe}_3\text{O}_4@\text{PLA}$, Fig. 1b) in the simulations, which was inserted inside the reactor with the geometry tools available in COMSOL. The fluid velocity profile and the distribution of concentrations of OFX in the reactor were determined by simultaneously solving the differential equations involved in the variation of the velocity, pressure, and concentration of pollutant with time and space.

The fluid (water) was assumed to be incompressible (constant den-

sity), Newtonian (constant viscosity) and under a laminar regime, such that the Navier–Stokes equations are valid (Temam, 2001). The velocity magnitude at the inlet of the reactor (v_{inlet}) was calculated according to

$$v_{inlet} = \frac{Q}{\pi r_{inlet}^2} \quad (1)$$

where Q is the flow rate (0.25 mL/min), and r_{inlet} is the radius of the inlet of the reactor (1.7 mm). The pressure at the outlet of the reactor was equal to the atmospheric pressure.

The variation in the concentration of OFX in the fluid was computed using the convection-diffusion equation coupled to an additional term that considers the degradation reaction of OFX (Hu, 2012). In this sense, the value reported in the literature ($2.033 \times 10^{-6} \text{ cm}^2/\text{s}$) was used for the diffusion coefficient of OFX in water (Solangi et al., 2022). The chemical degradation of the pollutant is supposed to take place only inside of the domain defined by the monolith. In addition, as found in the literature (Du et al., 2020; Jin et al., 2017; Tian et al., 2020), the oxidation process is assumed to be under kinetic control and constant concentrations of both catalyst and oxidant. Hence, pseudo-first-order kinetics can be considered, and an *effective* pseudo-first order rate constant can be defined. The concentrations of OFX at the different spatial points of the reactor outlet were averaged to calculate the concentration of the outflow solution at different times.

3. Results

3.1. Catalyst characterization

Thermograms of printed prototypes (Fig. 3a) reveal the presence of a glass transition temperature (T_g), cold crystallization temperature (T_{cc}) and melting temperature (T_m), which is indicative of a semicrystalline polymer. A reduction in T_{cc} enthalpy and an increase in T_{cc} are observed for the magnetic monolith. Those enthalpies were 24.1 and 16.2 J/g for the @PLA and 15- Fe_3O_4 @PLA reactors, respectively. This makes sense, given that the presence of a crystalline material in the blend makes PLA less prone to rearrangement and crystallization and requires more time for cold crystallization, showing a displacement in T_{cc} and a decrease in T_{cc} enthalpy. The decrease in cold crystallization enthalpy values also corresponded with a decrease in the melting enthalpy with the same trend, resulting in a crystallinity degree of 0 % (Ma et al., 2020). In other way, the high printing temperatures ($\approx 200^\circ\text{C}$) might affect the structure of the previously synthesized iron oxide particles, which can partially evolve to the $\gamma\text{-Fe}_2\text{O}_3$ structure (Anupama et al., 2017). Thus, the iron environment was characterized by Mössbauer spectroscopy in the printed monolith, as shown in Fig. 3b. The spectrum reveals the presence of two sextets associated with Fe_3O_4 , corresponding to iron in tetrahedral and octahedral positions. The hyperfine fields and isomer shift associated with each position are measured as 44.4 T (IS = 0.388 mm/s) and 48.5 T (IS = 0.321 mm/s), respectively. These hyperfine fields are slightly lower than the values expected for macroscopic-sized Fe_3O_4 (Greenwood, 2012), confirming the nanoscale nature of our composite and the absence of iron impurities.

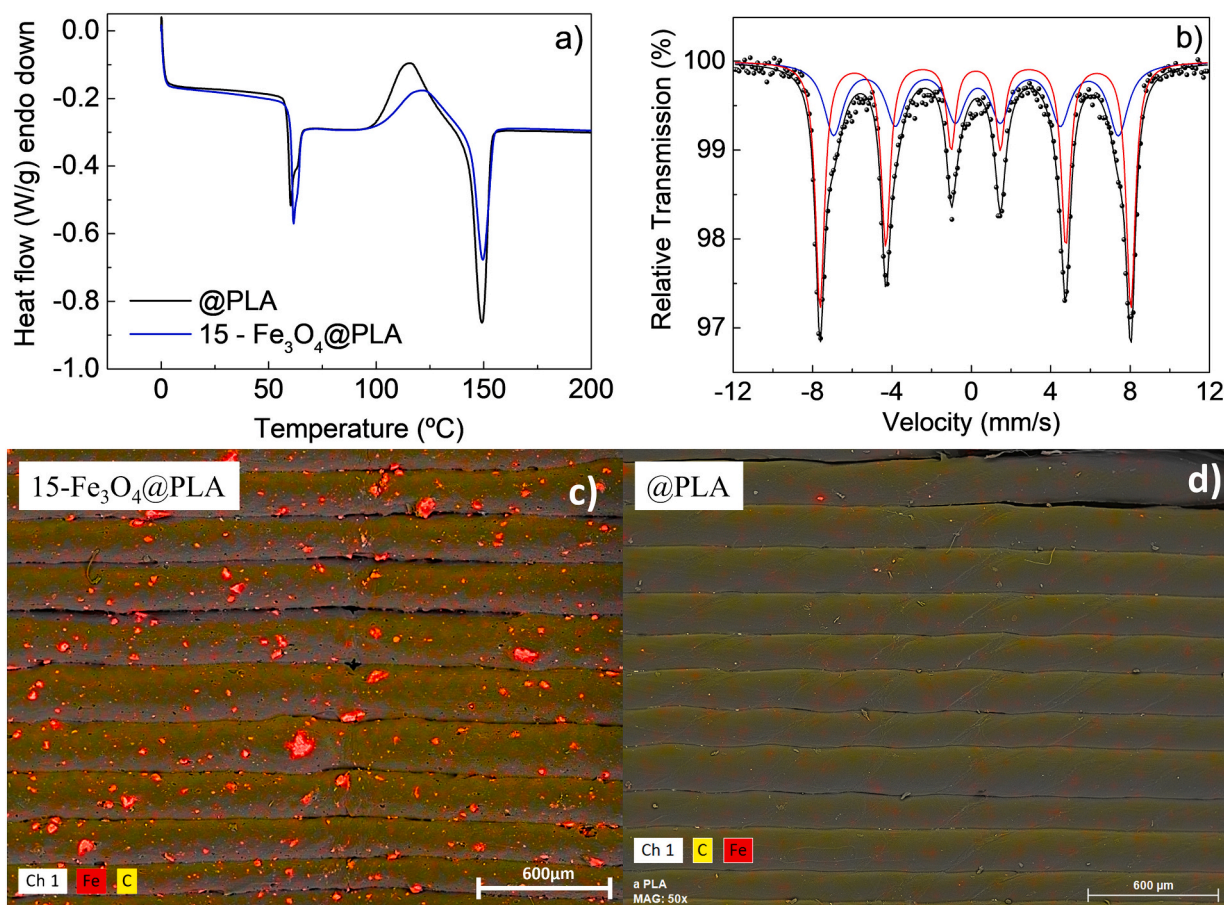


Fig. 3. a) DSC thermograms measured for 15- Fe_3O_4 @PLA and @PLA, b) Mössbauer spectrum of 15- Fe_3O_4 @PLA single monolith at room temperature. Dots are experimental data; red line is Fe in tetrahedral position and blue in the octahedral one. The combined spectrum of both iron positions is shown as a continuous black line, c) SEM elemental mapping image of the Fe and C elements of the as-printed 15- Fe_3O_4 @PLA monoliths and, d) control @PLA.

Typical merged element maps of C and Fe are shown in the SEM image of Fig. 3. The presence of many Fe particles embedded in the printed prototypes is evident. The distribution of the Fe particles is observed to be homogeneous along the entire analyzed surface. EDX analysis of 15-Fe₃O₄@PLA reveals an Fe content of 4.55 wt%. To demonstrate the uniformity of the Fe concentration across the reactor length, ICP measurements were performed in the top, center and bottom sections of the reactor. The values of Fe are 9.2, 10 and 9.8 wt%. This resulted in an average Fe concentration of 9.7 % (0.3), confirming a good dispersion of Fe in the longitudinal cross-section of the reactor. According to the stoichiometry of the nanoparticles used (Fe₃O₄) in the initial powder printing mixture, the magnetite content is 13.4 %. Considering the water physisorbed in magnetite, typically approximately 10 %, based on thermogravimetric analysis, this value is very close to the original value of 15 %.

3.2. Catalyst performance

3.2.1. Optimization of the SPS dose

As previously mentioned, the ratio [pollutant]/[oxidant] is a key factor that determines the process efficiency. Because SPS participates in parallel reactions that do not produce the active species (sulfate radicals mainly), particularly through a scavenging effect, the dosage used must be optimized. Therefore, the SPS feed concentration was varied in the range of 0.25–1.0 mM. In addition, blank experiments were performed to test the potential contribution to OFX removal of the @PLA support either by degradation via a noncatalytic reaction by SPS or by adsorption on the surface of the support. These results are presented in Fig. 4.

First, Fig. 4 shows that for the lower dose of oxidant (0.25 mM), OFX removal under steady state is only approximately 20 %, and the conversion increases for 0.5 mM and 1 mM doses of SPS, being 42 % and 55 %, respectively. Otherwise, a reduction in OFX concentration is observed in blank experiments via thermal activation of SPS in the presence of the @PLA support (3D-printed monolith without catalyst). The blank degradation for increasing SPS concentrations is 4, 13 and 27 %. Consequently, for a 1.0 mM SPS feed, the ratio between catalyst conversion and blank conversion decreases in comparison with lower SPS concentrations. In any case, for 1 mM SPS, the greatest degradation is observed compared to lower SPS doses. Additionally, considering the catalyst concentration effect and the fixed-bed reactor analysis (see below), 1 mM SPS is selected as the optimum concentration.

The degradation performance of monolith 15-Fe₃O₄@PLA was also

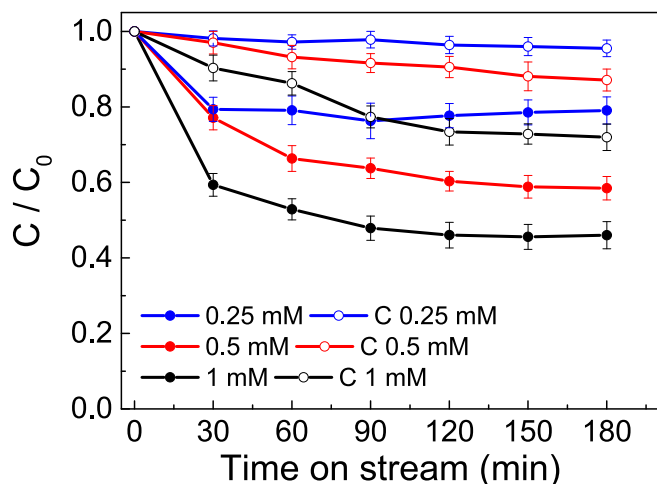


Fig. 4. Degradation performance of the catalyst 15-Fe₃O₄@PLA on the removal of OFX at varied SPS concentrations (0.25 mM – 0.5 mM – 1 mM - filled). Conditions: flow rate = 0.25 mL/min, [OFX]₀ = 1 mg/L, pH₀ = 5, T = 40 °C. Blank analysis with @PLA support is performed in the same experimental conditions (unfilled).

studied by computational fluid dynamics simulations (see Section 2.6). The influence of the concentration of SPS was inserted on the value of the effective pseudo-first-order rate constant of the degradation of OFX (k_{rate}), which takes into account both the catalytic and noncatalytic oxidation of OFX and its adsorption on the PLA support.

Fig. 5 depicts the results obtained from the simulations, comparing them with the experimental curves. The simulations predict the same tendency as that observed experimentally, with an initial quasilinear decrease in the concentration followed by a stabilization of the c/c_0 ratio at long times (steady state). The optimum values for the effective rate constant (shown on the plots) can be estimated by minimizing the discrepancies between the experimental and simulated data in the steady state region. Note that, except for the lower concentration of SPS, the transient region at low times cannot be fitted correctly, and many discrepancies are observed. This fact is a consequence of using a single value for the rate constant, whereas the conversion rate changes with time until the steady state is reached.

The concentration distribution of OFX in the reactor under steady-state conditions is shown in Fig. 6 for the three assayed concentrations of SPS. Homogeneous concentrations are found in the lower half of the reactor and are equal to the concentration at the inlet of the reactor ($c_0 = 1 \text{ mg/L} = 2.77 \times 10^{-3} \text{ mol/m}^3$). Once the fluid crosses the monolith, the degradation reaction causes a gradual decrease in the concentrations until a minimum value is reached at the outlet of the cell. Note that initial values are again attained at the top of the reactor. This behavior is a consequence of the low velocity of the fluid in this region, since the existence of a physical wall in the normal direction of the flow causes the accumulation of OFX and the increment of the concentration (see Fig. 7).

3.2.2. Evaluation of the Catalyst conformation

The use of a cylinder-shaped hollow catalyst degraded approximately 55 % of the target pollutant under the tested conditions. In an effort to improve the efficiency of the 3D reactors, we prepared larger monoliths (L = 30 mm) with a meshed configuration (Fig. 1e). In particular, fluid dynamics play a very important role given that the operations are conducted at very low flow rates, driving the fluids to a laminar regime, which significantly hampers the interaction between reactants. In contrast, higher regimes will promote both mixing and reaction, but they significantly affect the pollutant's residence time inside the reactor. Therefore, it is important to create both turbulence and mixing while operating with very low fluid velocities. One possibility is

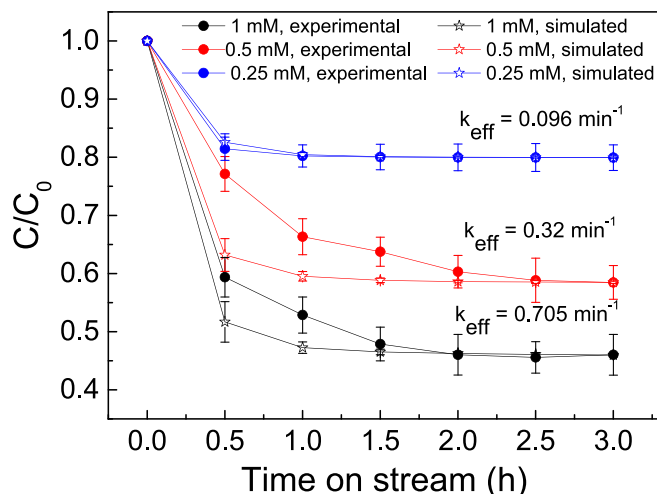


Fig. 5. Simulated (unfilled stars) and experimental (filled dots) variation of the concentration of OFX on the out-flow solution with time on the 15-Fe₃O₄@PLA-reactor. The optimum effective rate (k_{eff}) constants that minimize the differences between experimental and simulated data at long times are shown on the plot.

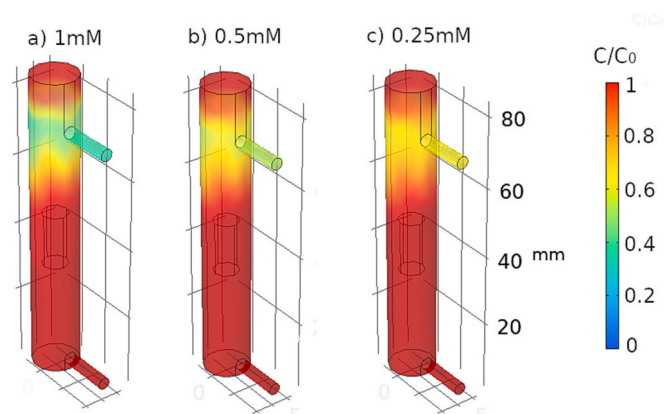


Fig. 6. Computed distribution of the C/C_0 ratio of OFX on the reactor equipped with 15- Fe_3O_4 @PLA monolith at the different concentrations of SPS under steady state conditions.

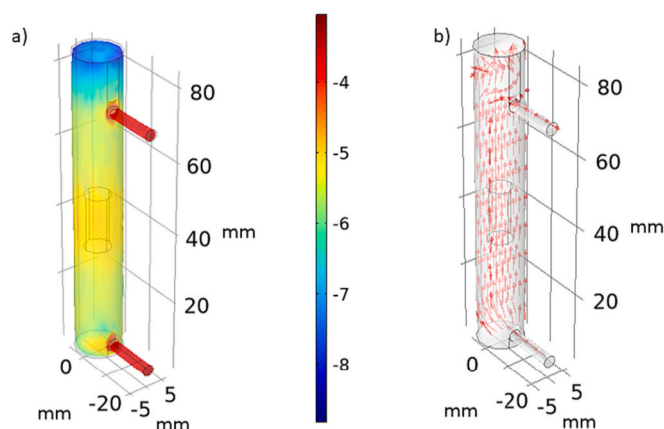


Fig. 7. a) Velocity profiles computed on the reactor equipped with 15- Fe_3O_4 @PLA monolith under steady state conditions. The values plotted correspond to the logarithmic of the magnitude of velocity of the fluid in m/s, b) Arrow plot representing the velocity vectors of the fluid along the reactor. The intensity of the colour of the arrows reflects the magnitude of the velocity.

to place obstacles in the fluid path and thus eliminate the preferential paths.

The effect of the new double mesh configuration on OFX degradation is compared with that of the single catalyst using the optimized conditions established previously (see Fig. 8). For comparison, the control degradation performance of the new double mesh prototype (@PLA-DM) is also depicted. At first sight, there is an improvement in the degradation, with a value of 82 % pollutant removal compared to the simple catalyst (55 %). In a simple way, this result can be explained by both the increment of the residence time because of the new length and contact surface of the catalyst and the increase in iron oxide. Furthermore, two other facts are noteworthy: the reproducibility of the results along the testing time and the short time to obtain steady-state conditions. Both contributions make sense with the fluid dynamic improvement.

3.2.3. 3D printed 15- Fe_3O_4 @PLA-DM: long-term stability

Once the degradation process and the design of the 3D printing prototype that improves the fluid dynamics have been optimized, a long-term continuous experiment was conducted. The obtained results are illustrated in Fig. 9. Additional blank experiments were performed to test the potential contribution to OFX removal either by degradation via a noncatalytic reaction by SPS or by adsorption on the surface of the catalyst. The oxidation of OFX by SPS in the absence of magnetite in the

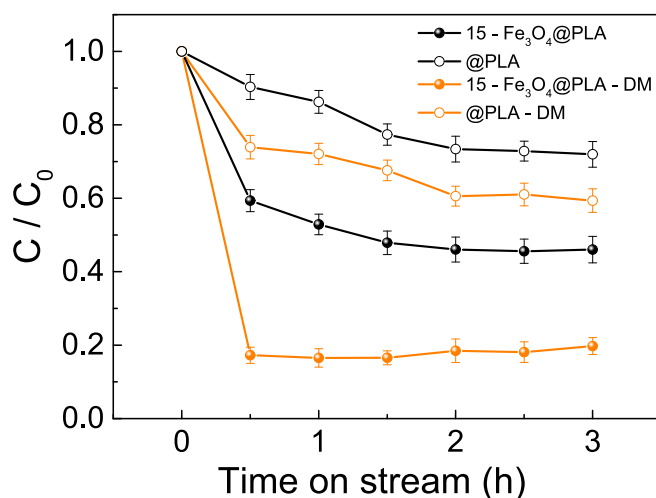


Fig. 8. Degradation performance of the simple catalyst 15- Fe_3O_4 @PLA and 15- Fe_3O_4 @PLA - DM on the removal of OFX. Conditions: (flow rate = 0.25 mL/min, $[\text{SPS}]_0 = 1 \text{ mM}$, $[\text{OFX}]_0 = 1 \text{ mg/L}$, $\text{pH}_0 = 5$, $T = 40^\circ \text{C}$). Blank analysis with @PLA and @PLA - DM support are performed in the same experimental conditions (unfilled).

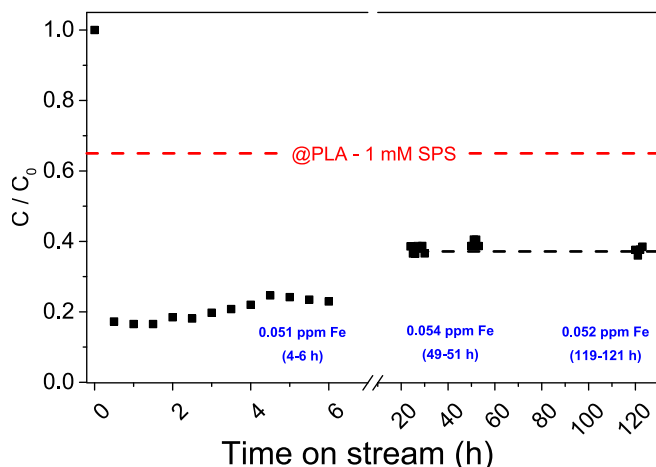


Fig. 9. Long-term performance of the catalyst 15- Fe_3O_4 @PLA-DM on the degradation of OFX (flow rate = 0.25 mL/min, $[\text{OFX}]_0 = 1 \text{ mg/L}$, $[\text{SPS}]_0 = 1 \text{ mM}$, $\text{pH}_0 = 5$, $T = 40^\circ \text{C}$).

@PLA - DM support is represented by the dashed red line shown in Fig. 9, and its effect is not negligible. Approximately 35 % of OFX oxidation is attributed to the reaction with SPS. Otherwise, the adsorption of OFX on the @PLA - DM support is insignificant during the experiments performed in the absence of SPS. Similarly, the 15- Fe_3O_4 @PLA - DM catalyst is stable for up to 3 h, and a significant decrease in efficiency is observed for up to 1 day of operation. Thereafter, the catalyst exhibits a constant activity until 120 h of streaming time, without any loss of activity being observed in this interval. In accordance with this period of constant activity, the dissolved iron concentration is almost insignificant over the long-term continuous experiment (0.051–0.054 ppm). The total iron leached after 120 h on-stream represents less than 0.036 wt% of the Fe content of the double mesh printed reactor (0.0972 mg).

Although the efficiency of the degradation process is improved with the double mesh monolith, complete degradation has not yet been achieved. An alternative approach can be printing wider and taller monoliths with the idea of increasing the surface contact with the contaminated solution, although this can result in poor reproducibility

of the printing quality. An easier approach, relying on the benefits of 3D printing, is to generate pellets of a given size, so that iron oxide nanoparticles are well supported in the PLA to be later fragmented into smaller sizes and used in a packed bed reactor. In this approach, we have on the one hand, the advantages of the anchorage of the catalyst on the support and, on the other hand, an increase in the active area in the packaged process because it is constituted by reduced fragments.

3.2.4. 3D printed pellets: degradation in a fixed-bed reactor

As mentioned in Section 2.4, the packed reactor was prepared using printed micropellets in the range of 125–200 μm . Fig. 10a depicts an SEM image of the micropellets, showing that they present similar sizes, ranging between 100 and 200 μm . In Fig. 10b, the EDX analysis of the Fe content is presented, which corroborates the homogeneous Fe distribution along the analyzed surface. To obtain more insights into the morphology of the micropellet surface after the milling process, Fig. 10c shows a high-resolution SEM image of one micropellet, where the Fe_3O_4 aggregates are clearly observed. Finally, the micropellet size distribution measured by laser diffraction (LD) shows a mean pellet diameter of 158 μm . Although there is a weak contribution between 2 and 40 μm , the main portion of the packed sample comprises fragments between 125 and 200 μm , as expected.

AOP using a fixed-bed reactor was performed with the optimized conditions described in the previous sections. To assess the real degradation efficiency of the micropellets packed in the reactor, both control experiments (adsorption and degradation) were performed (see Fig. 11). Briefly, adsorption was assessed in the glass reactor with packed micropellets before oxidant addition such that there was a contribution

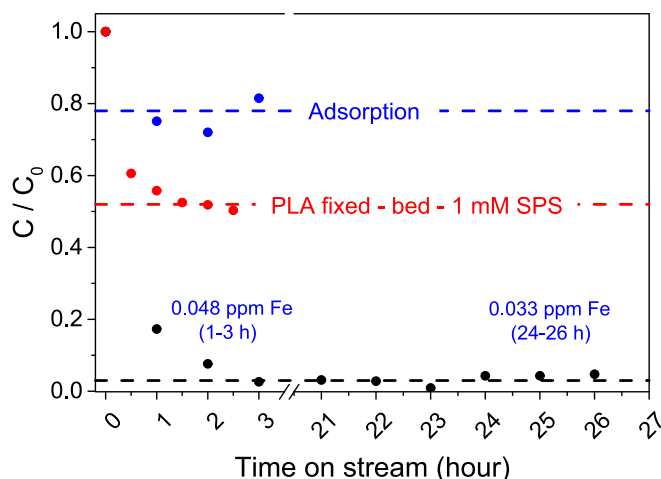


Fig. 11. Long-term performance of the fixed-bed reactor upon AOP of OFX (flow rate = 0.25 mL/min, $[\text{OFX}]_0 = 1 \text{ mg/L}$, $[\text{SPS}]_0 = 1 \text{ mM}$, $\text{pH}_0 = 5$, $T = 40^\circ\text{C}$).

of both Fe_3O_4 particles and the PLA on which the particles are embedded. This adsorption contribution was confirmed because of the increase in the effective area in the packed reactor, reducing the concentration of the pollutant by 20 %, whereas it is not observed in the printed monoliths. Degradation tests, as previously described, were performed by packing 1 g of only PLA micropellets with a size fraction

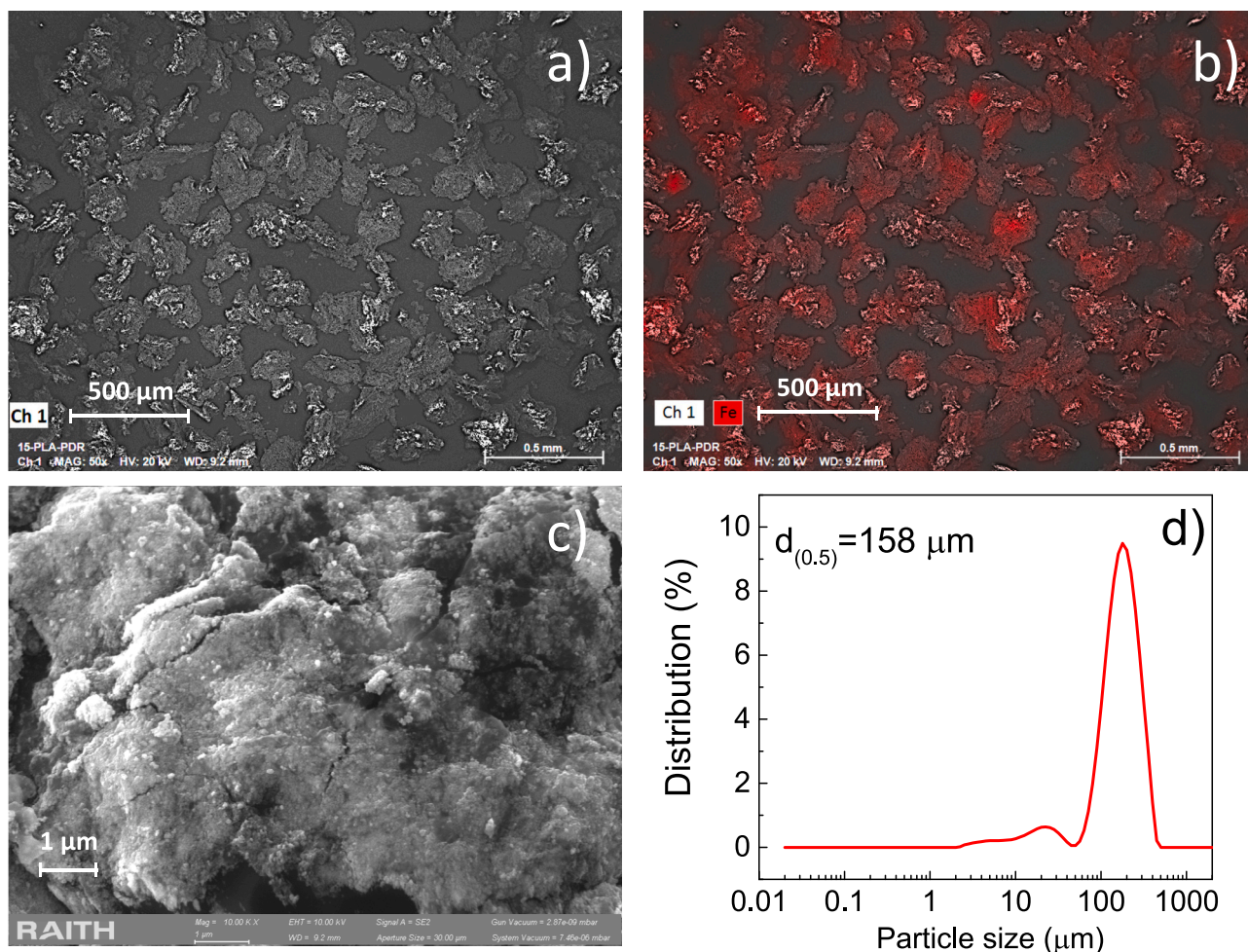


Fig. 10. a) and c) SEM image, b) Fe-EDX image, and d) micropellet size distribution.

between 125 and 200 μm in the glass tube. The degradation process was subjected to the same conditions previously optimized, resulting in a decrease of approximately 50 % in pollutant concentration. Finally, the black dots in Fig. 11 represent the degradation occurring in the fixed-bed reactor with $\text{Fe}_3\text{O}_4@\text{PLA}$ micropellets during 26 h of operation. The initial concentration of 1 mg/L is decreases to values below 50 ppb (according to current legislation) then remains unchanged, at least within the tested time period. In addition, the stability of the catalyst was assessed against the leached concentration of Fe measured by ICP-OES in the outflow reactor. The measured doses at 1–3 h of operation and after one day are 0.048 and 0.033 ppm, respectively, which are not enough to consider a homogeneous contribution to degradation or a potential toxicity source. In fact, the leached iron is far from the median iron concentration in rivers and drinking water which has been described by the WHO as 0.7 and 0.3 ppm, respectively (World Health Organization, n.d.-a, n.d.-b). Higher doses can be toxic because it forms radical oxygen species that could damage tissues. Also, there are several studies of the relation between a high presence of iron in humans and the development of some aging diseases such as Atherosclerosis and Alzheimer (Brewer, 2010). Recent studies have been reported in the literature for OFX degradation in packed reactors. For instance, Li et al. assessed the degradation of OFX in distilled water together with other contaminants in a packed bed constituted by CuO particles, obtaining a total degradation efficiency over the 0.250 ppm initial concentration, albeit with a pellet loading of 140 g (Li et al., 2022a). In addition, some Cu leaching (0.35–0.37 ppm) is observed within the operation time of 1 to 4 h. On the other hand, 3D printing technology demonstrates the enhanced fixation of the active sites to the support, either in the monolith prints or in the assembly of the packed bed of printed fragments. It is well known the mass transfer limitation observed when considered heterogeneous catalyst to its homogeneous counterpart (Ortiz de la Plata et al., 2010). As the lifetime of radicals $\cdot\text{OH}$ and $\text{SO}_4^{\cdot-}$ in water, is extremely short, the concentration in the bulk aqueous phase, where most of the reaction occurs, is much lower than that on the surface of catalysts where radicals are produced. One strategy to minimize the mass transfer limitation of short-lived species is to design the system under spatial confinement; that is, restrict the space where the reaction occurs such that the distance between the “bulk” and “catalyst surface” is set to be below a certain length scale. For that reason, the degradation improvement in fixed-bed reactor experiment in comparison to monoliths it is not only an effect of the larger active area, and the adsorption effect shown (Zhang et al., 2023), but also because of the reduced space between the catalyst surface where de radicals are generated and the bulk solution passing through all the confined space (Zhang et al., 2020).

Thus opens the possibility to handle a larger flow of polluted solution merely by enlarging the bed length, pellet composition, or flow rate and to enlarge the AOP performance based on spatial confinement.

4. Conclusion

Three 3D printed monoliths with varied geometries were prepared from a mixture of iron oxide nanoparticles and polylactic acid powder at 15 wt% iron oxide. The design of the monoliths was carefully adjusted to study the effect on the removal efficiency of the antibiotic ofloxacin (OFX). First, a simple cylindrical monolith was created, followed by a double-size cylindrical monolith with an internal mesh. Finally, micropellets ranging between 125 and 200 μm were used to pack a fixed-bed reactor.

The effect of the SPS dose was first evaluated with a simple monolith. By fixing the temperature at 40 $^{\circ}\text{C}$, the initial concentration of OFX at 1 mg/L, the pH value at 5 and the flow rate at 0.25 mL/min, increasing the SPS dose from 0.25 mM to 1 mM modified the antibiotic removal from 22 to 55 %. Computational fluid dynamics simulations were carried out under these conditions, allowing for a determination of the velocity and concentration profile inside the reactor and estimation of values for the effective pseudo-first-order rate constants for the degradation of OFX.

Afterward, the degradation performance of the double mesh and the fixed-bed reactor was evaluated at the optimized dose of 1 mM SPS. The geometry of the scaffolds significantly influenced the performance of the catalytic systems evaluated. An increase in the space time because of the greater length of the double mesh catalyst yielded a conversion value of 82 %. In addition, the internal mesh modifies the fluid dynamics of the system, enduring an ideal mixture of reactants. It is important to highlight that all prototypes suffer a slight deactivation due to iron leaching. Finally, new possibilities are proposed using fixed-bed reactors based on 3D printed micropellets. Here, by notably increasing the active area, ofloxacin is completely degraded. Therefore, this 3D approach overcomes some of the most important limitations in the advanced oxidation technology field while ensuring low cost, continuous flow operation, long-term catalytic stability and feasibility of application on a larger scale.

CRedit authorship contribution statement

S. Fernandez-Velayos: Investigation, Methodology. **G. Vergara:** Investigation, Methodology. **J.M. Olmos:** Writing – review & editing. **J. Sanchez-Marcos:** Supervision, Writing – review & editing. **N. Menendez:** Supervision, Writing – review & editing. **P. Herrasti:** Resources, Supervision, Project administration, Funding acquisition, Writing – review & editing. **E. Mazarío:** Writing – original draft, Writing – review & editing, Visualization, Conceptualization, Supervision, Resources, Project administration, Funding acquisition.

Declaration of competing interest

The authors declare that they have no known competing financial interests or personal relationships that could have appeared to influence the work reported in this paper.

Data availability

Data will be made available on request.

Acknowledgments

This research has been supported by the Spanish Ministry of Science and Innovation through the project PID2021-123431OB-I00.

References

- Acuña-Bedoya, J.D., Rangel-Sequeda, J.F., Loreda-Cancino, M., Maya-Treviño, M. de L., Domínguez-Jaimes, L.P., Hernández-López, J.M., 2022. Integration of the adsorption and electro-oxidation process using 3D printed activated carbon monoliths for the degradation of pharmaceutical compounds. *J. Environ. Chem. Eng.* 10, 108203. <https://doi.org/10.1016/j.jece.2022.108203>.
- Alam, M.-U., Ferdous, S., Ercumen, A., Lin, A., Kamal, A., Luies, S.K., Sharior, F., Khan, R., Rahman, M.Z., Parvez, S.M., Amin, N., Tadesse, B.T., Moushomi, N.A., Hasan, R., Taneja, N., Islam, M.A., Rahman, M., 2021. Effective treatment strategies for the removal of antibiotic-resistant bacteria, antibiotic-resistance genes, and antibiotic residues in the effluent from wastewater treatment plants receiving municipal, hospital, and domestic wastewater: protocol for a S. JMIR Res. Protoc. 10, e33365 <https://doi.org/10.2196/33365>.
- Anupama, A.V., Keune, W., Sahoo, B., 2017. Thermally induced phase transformation in multi-phase iron oxide nanoparticles on vacuum annealing. *J. Magn. Magn. Mater.* 439, 156–166. <https://doi.org/10.1016/j.jmmm.2017.04.094>.
- Brand, R.A., 1987. Improving the validity of hyperfine field distributions from magnetic alloys. *Nucl. Instruments Methods Phys. Res. Sect. B Beam Interact. Mater. Atoms* 28, 398–416.
- Brewer, G.J., 2010. Risks of copper and Iron toxicity during aging in humans. *Chem. Res. Toxicol.* 23, 319–326. <https://doi.org/10.1021/tx900338d>.
- Bungau, S., Tit, D.M., Behl, T., Aleya, L., Zaha, D.C., 2021. Aspects of excessive antibiotic consumption and environmental influences correlated with the occurrence of resistance to antimicrobial agents. *Curr. Opin. Environ. Sci. Heal.* 19, 100224. <https://doi.org/10.1016/j.coesh.2020.10.012>.
- Cao, Q., Lou, F., Liu, N., Zhang, J., Wu, L., 2021. Continuous catalytic ozonation of antibiotics using Mn and Cu oxides on $\gamma\text{-Al}_2\text{O}_3$ pellets in a micropacked bed reactor. *ACS ES&T Water* 1, 1911–1920. <https://doi.org/10.1021/acsestwater.1c00141>.

- Deng, Y., Debognies, A., Zhang, Q., Zhang, Z., Zhou, Z., Zhang, J., Sun, L., Lu, T., Qian, H., 2022. Effects of ofloxacin on the structure and function of freshwater microbial communities. *Aquat. Toxicol.* 244, 106084.
- Du, Z., Li, K., Zhou, S., Liu, X., Yu, Y., Zhang, Yunhai, He, Y., Zhang, Yongjun, 2020. Degradation of ofloxacin with heterogeneous photo-Fenton catalyzed by biogenic Fe-Mn oxides. *Chem. Eng. J.* 380, 122427. <https://doi.org/10.1016/j.cej.2019.122427>.
- Fernández-Velayos, S., Sánchez-Marcos, J., Muñoz-Bonilla, A., Herrasti, P., Menéndez, N., Mazarío, E., 2021. Direct 3D printing of zero valent iron@polylactic acid catalyst for tetracycline degradation with magnetically inducing active persulfate. *Sci. Total Environ.* 150917.
- Fernández-Velayos, S., Menéndez, N., Herrasti, P., Mazarío, E., 2023. Ofloxacin degradation over nanosized Fe₃O₄ catalyst via thermal activation of persulfate ions. *Catalysts*. <https://doi.org/10.3390/catal13020256>.
- Gallo-Cordova, A., Castro, J.J., Winkler, E.L., Lima, E., Zysler, R.D., Morales, M. del P., Ovejero, J.G., Streitwieser, D.A., 2021. Improving degradation of real wastewaters with self-heating magnetic nanocatalysts. *J. Clean. Prod.* 308, 127385. <https://doi.org/10.1016/j.jclepro.2021.127385>.
- Greenwood, N.N., 2012. *Mössbauer Spectroscopy*. Springer Science & Business Media.
- Gupta, A., Garg, A., 2019. Adsorption and oxidation of ciprofloxacin in a fixed bed column using activated sludge derived activated carbon. *J. Environ. Manage.* 250, 109474. <https://doi.org/10.1016/j.jenvman.2019.109474>.
- Hu, H.H., 2012. In: Kundu, P.K., Cohen, I.M., Dowling, D.R.B.T.-F.M., Fifth E (Eds.), Chapter 10 - computational fluid dynamics. Academic Press, Boston, pp. 421–472. <https://doi.org/10.1016/B978-0-12-382100-3.10010-1>.
- Jandyal, A., Chaturvedi, I., Wazir, I., Raina, A., Ul Haq, M.I., 2022. 3D printing – a review of processes, materials and applications in industry 4.0. *Sustain. Oper. Comput.* 3, 33–42. <https://doi.org/10.1016/j.susoc.2021.09.004>.
- Jin, H., Tian, X., Nie, Y., Zhou, Z., Yang, C., Li, Y., Lu, L., 2017. Oxygen vacancy promoted heterogeneous Fenton-like degradation of Ofloxacin at pH 3.2–9.0 by Cu substituted magnetic Fe₃O₄@FeOOH nanocomposite. *Environ. Sci. Technol.* 51, 12699–12706. <https://doi.org/10.1021/acs.est.7b04503>.
- Kanakaraju, D., Glass, B.D., Oelgemöller, M., 2018. Advanced oxidation process-mediated removal of pharmaceuticals from water: a review. *J. Environ. Manage.* 219, 189–207. <https://doi.org/10.1016/j.jenvman.2018.04.103>.
- Lee, J., von Gunten, U., Kim, J.-H., 2020. Persulfate-based advanced oxidation: critical assessment of opportunities and roadblocks. *Environ. Sci. Technol.* 54, 3064–3081. <https://doi.org/10.1021/acs.est.9b07082>.
- Li, C., de Melo Costa Serge, N., Nogueira, R.F.P., Chiron, S., Goetz, V., 2022a. Peroxydisulfate activation by CuO pellets in a fixed-bed column, operating mode and assessments for antibiotics degradation and urban wastewater disinfection. *Environ. Sci. Pollut. Res.* 29, 71709–71720. <https://doi.org/10.1007/s11356-022-20847-1>.
- Li, T., Lu, S., Lin, W., Ren, H., Zhou, R., 2022b. Heat-activated persulfate oxidative degradation of ofloxacin: kinetics, mechanisms, and toxicity assessment. *Chem. Eng. J.* 433, 133801.
- Liu, X., Huang, F., Yu, Y., Zhao, P., Zhou, Y., He, Y., Xu, Y., Zhang, Y., 2019. Ofloxacin degradation over Cu–Ce tyre carbon catalysts by the microwave assisted persulfate process. *Appl. Catal. Environ.* 253, 149–159. <https://doi.org/10.1016/j.apcatb.2019.04.047>.
- Liu, X., Liu, Y., Lu, S., Wang, Z., Wang, Y., Zhang, G., Guo, X., Guo, W., Zhang, T., Xi, B., 2020a. Degradation difference of ofloxacin and levofloxacin by UV/H₂O₂ and UV/PS (persulfate): efficiency, factors and mechanism. *Chem. Eng. J.* 385, 123987.
- Liu, G., Zhang, Y., Yu, H., Jin, R., Zhou, J., 2020b. Acceleration of goethite-catalyzed Fenton-like oxidation of ofloxacin by biochar. *J. Hazard. Mater.* 397, 122783. <https://doi.org/10.1016/j.jhazmat.2020.122783>.
- Lozano, I., López, C., Menéndez, N., Casillas, N., Herrasti, P., 2018. Design, construction and evaluation of a 3D printed electrochemical flow cell for the synthesis of magnetite nanoparticles. *J. Electrochem. Soc.* 165, H688–H697.
- Ma, B., Zhang, H., Wang, K., Xu, H., He, Y., Wang, X., 2020. Influence of scPLA microsphere on the crystallization behavior of PLLA/PDLA composites. *Compos. Commun.* 21, 100380. <https://doi.org/10.1016/j.coco.2020.100380>.
- Nasr Esfahani, K., Zandi, M.D., Travieso-Rodríguez, J.A., Graells, M., Pérez-Moya, M., 2021. Manufacturing and application of 3D printed photo Fenton reactors for wastewater treatment. *Int. J. Environ. Res. Public Health* 18. <https://doi.org/10.3390/ijerph18094885>.
- Nieto-Sandoval, J., di Luca, C., Gomez-Herrero, E., Inchaurredo, N., Muñoz, M., de Pedro, Z.M., Casas, J.A., 2021. Innovative iron oxide foams for the removal of micropollutants by catalytic wet peroxide oxidation: assessment of long-term operation under continuous mode. *J. Environ. Chem. Eng.* 9, 105914. <https://doi.org/10.1016/j.jece.2021.105914>.
- Ortiz de la Plata, G.B., Alfano, O.M., Cassano, A.E., 2010. Decomposition of 2-chlorophenol employing goethite as Fenton catalyst. I. Proposal of a feasible, combined reaction scheme of heterogeneous and homogeneous reactions. *B. Environ.* 95, 1–13. <https://doi.org/10.1016/j.apcatb.2009.12.005>.
- Quintanilla, A., Carbajo, J., Casas, J.A., Miranzo, P., Osendi, M.I., Belmonte, M., 2020. Graphene-based nanostructures as catalysts for wet peroxide oxidation treatments: from nanopowders to 3D printed porous monoliths. *Catal. Today* 356, 197–204. <https://doi.org/10.1016/j.cattod.2019.06.026>.
- Sayed, M., Gul, M., Shah, N.S., Khan, J.A., Khan, Z.U.H., Rehman, F., Khan, A.R., Rauf, S., Arandiyani, H., Yang, C.P., 2019. In-situ dual applications of ionic liquid coated Co²⁺ and Fe³⁺ co-doped TiO₂: superior photocatalytic degradation of ofloxacin at pilot scale level and enhanced peroxidase like activity for calorimetric biosensing. *J. Mol. Liq.* 282, 275–285. <https://doi.org/10.1016/j.molliq.2019.03.022>.
- Solangi, N., Kumar, J., Naz, G., Soomro, R.A., 2022. The preparation of NiCo2O₄ nanoboulders and their application in the electrochemical detection of ofloxacin drug. *J. CIS Open* 6, 100054. <https://doi.org/10.1016/j.jciso.2022.100054>.
- Temam, R., 2001. *Navier-Stokes Equations: Theory and Numerical Analysis*. AMS/Chelsea publication, AMS Chelsea Pub.
- Tian, Y., He, X., Chen, W., Tian, X., Nie, Y., Han, B., Lin, H.-M., Yang, C., Wang, Y., 2020. Significant enhancement of photo-Fenton degradation of ofloxacin over Fe-Dis@Sep due to highly dispersed FeC₆ with electron deficiency. *Sci. Total Environ.* 723, 138144. <https://doi.org/10.1016/j.scitotenv.2020.138144>.
- Varela, A.R., André, S., Nunes, O.C., Manaia, C.M., 2014. Insights into the relationship between antimicrobial residues and bacterial populations in a hospital-urban wastewater treatment plant system. *Water Res.* 54, 327–336. <https://doi.org/10.1016/j.watres.2014.02.003>.
- World Health Organization, n.d.-a Access, watch, Reserve classification of antibiotics for evaluation and monitoring of use 2021 [WWW Document]. URL <https://www.who.int/publications/i/item/2021-aware-classification>.
- World Health Organization, n.d.-b Chemical hazards in drinking-water [WWW Document]. URL <https://www.who.int/teams/environment-climate-change-and-health/water-sanitation-and-health/chemical-hazards-in-drinking-water>.
- Xie, Y., Yu, Y., Xie, H., Huang, F., Hughes, T.C., 2022. 3D-printed heterogeneous Cu₂O monoliths: reusable supports for antibiotic treatment of wastewater. *J. Hazard. Mater.* 436, 129170. <https://doi.org/10.1016/j.jhazmat.2022.129170>.
- Zhang, S., Sun, M., Hedtke, T., Deshmukh, A., Zhou, X., Weon, S., Elimelech, M., Kim, J.-H., 2020. Mechanism of heterogeneous Fenton reaction kinetics enhancement under nanoscale spatial confinement. *Environ. Sci. Technol.* 54, 10868–10875. <https://doi.org/10.1021/acs.est.0c02192>.
- Zhang, D., An, Z., Zhang, Y., Hu, Y., Zhan, J., Zhou, H., Wu, M., 2023. MoS₂@SiO₂ enhanced persulfate oxidation for the degradation of triazine herbicides in fixed-bed reactor. *J. Water Process Eng.* 52, 103523. <https://doi.org/10.1016/j.jwpe.2023.103523>.
- Zhu, L., Ji, J., Liu, J., Mine, S., Matsuoka, M., Zhang, J., Xing, M., 2020. Designing 3D-MoS₂ sponge as excellent Cocatalysts in advanced oxidation processes for pollutant control. *Angew. Chemie Int. Ed.* 59, 13968–13976. <https://doi.org/10.1002/anie.202006059>.